Bubble-Decorated Honeycomb-Like Graphene Film as Ultrahigh Sensitivity Pressure Sensors

Lizhi Sheng, Yuan Liang, Lili Jiang, Qian Wang, Tong Wei, Liangti Qu, and Zhuangjun Fan**

Recently, macroporous graphene monoliths (MGMs), with ultralow density and good electrical conductivity, have been considered as excellent pressure sensors due to their excellent elasticity with a rapid rate of recovery. However, MGMs can only exhibit good sensitivity when the strain is higher than 20%, which is undesirable for touch-type pressure sensors, such as artificial skin. Here, an innovative method for the fabrication of freestanding flexible graphene film with bubbles decorated on honeycomb-like network is demonstrated. Due to the switching effect depended on "point-to-point" and "point-to-face" contact modes, the graphene pressure sensor has an ultrahigh sensitivity of 161.6 kPa^{-1} at a strain less than 4%, several hundred times higher than most previously reported pressure sensors. Moreover, the graphene pressure sensor can monitor human motions such as finger bending and pulse with a very low operating voltage of 10 mV, which is sufficiently low to allow for powering by energy-harvesting devices, such as triboelectric generators. Therefore, the high sensitivity, low operating voltage, long cycling life, and large-scale fabrication of the pressure sensors make it a promising candidate for manufacturing low-cost artificial skin.

1. Introduction

Strain or pressure sensors, detecting the electrical shift upon mechanical deformation, have attracted much attention for applications in infrastructural and automobile health monitoring.[1–7] Especially, flexible pressure sensors with high sensitivity in low deformability (strain) are highly desirable for better emulating human skin[8–11] and more precisely capturing human motions.[1–3] Piezoresistive-type sensor, based on the change in the resistance of materials with mechanical deformation,[12,13] is a promising pressure sensor due to its simple fabrication, low cost, and easy signal collection.[14,15] Conventionally, flexible and stretchable rubbers filled with conductive carbon such as carbon black,[15] carbon nanotubes,[16,17] and graphene,[15] are used as sensing materials for piezoresistive sensors. However, these conductive rubber sensors often show poor sensitivity and high operated pressure (>10 kPa), limiting their further application in artificial skin.[14,18] To achieve a high sensitivity in the low-pressure regime (<10 kPa), aligned electrospun nanofibers in piezoelectric sensors,[19] microstructured polydimethylsiloxane (PDMS) in capacitive[2,18,20–22] and triboelectric sensors,[23,24] have been employed and developed. However, the high operating voltage for those devices (10–100 V) limits their real applications in wearable devices.[25]

Recently, macroporous graphene monoliths (MGMs), with ultralow density and good electrical conductivity, have aroused considerable recent interest toward pressure sensing due to their excellent elasticity with a rapid rate of recovery.[26,27] However, MGMs can exhibit better sensitivity when the strain is higher than 30%, which is undesirable for touch-type pressure sensors,[14] such as artificial skin. Thus, it is of great challenge for obtaining pressure sensors with high sensitivity at both low strain and pressure.

Here, we demonstrate a novel bubble-decorated honeycomb-like graphene film (BHGF) as flexible, highly sensitively pressure sensor for monitoring the body motion. Honeycomb-like network and the bubbles are derived from the evaporation of interlayer water and the evolved gases (H_2O, CO_2, and CO) trapped in adjacent graphene sheet during the pyrolysis of oxygen groups, respectively. Due to the switching effect depended on "point–to-point" and "point-to-face" contact modes, the BHGF pressure sensor has an ultrahigh sensitivity of 161.6 kPa^{-1}, several hundred times higher than most previously reported pressure sensors.[5,13,14,18,20] More importantly, the BHGF sensor exhibits a low operating voltage and good cycling stability at a very low strain less than 4%, demonstrating that it is very suitable for application in artificial skin.[28]

Dr. L. Sheng, Dr. L. Jiang, Dr. Q. Wang, Prof. T. Wei, Prof. Z. Fan
Key Laboratory of Superlight Materials and Surface Technology
Ministry of Education
College of Material Science and Chemical Engineering
Harbin Engineering University
Harbin 150001, China
E-mail: fanzhj666@163.com
Dr. Y. Liang, Prof. L. Qu
Key Laboratory of Cluster Science Ministry of Education
School of Chemistry
Beijing Institute of Technology
Beijing 100081, China
E-mail: lqu@bit.edu.cn

DOI: 10.1002/adfm.201502960

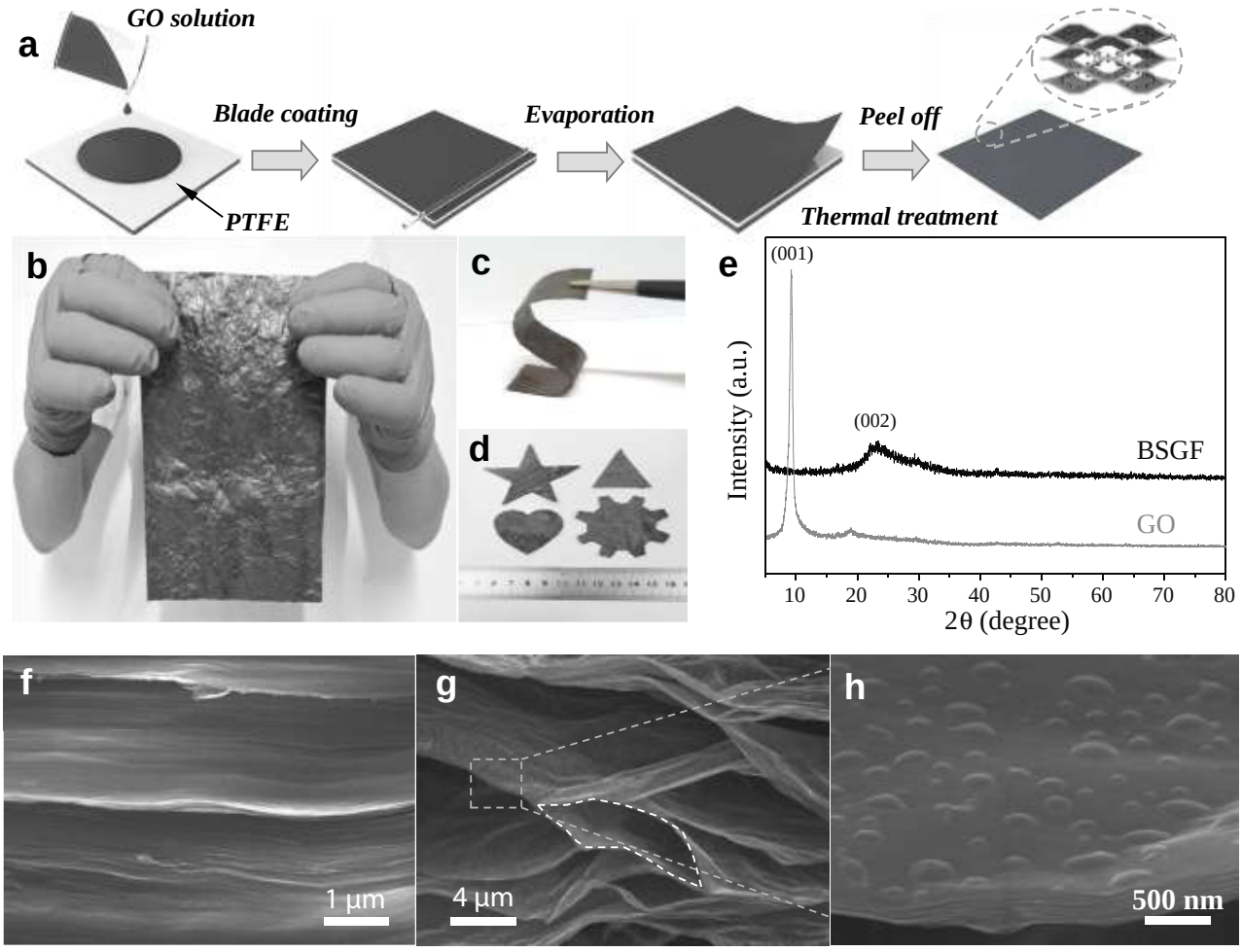

Figure 1. a) Schematic illustration of the preparation of the BHGF film. b) Digital photos of the BHGF film. c) Flexibility and d) different shapes of BHGF. e) XRD patterns of GO and BHGF. f) SEM image of GO film. g) Low and h) high-magnification SEM images of BHGF; the white dotted line is cell unit.

2. Results and Discussion

2.1. Material Synthesis and Structural Characterization

The formation of BHGF is schematically illustrated in **Figure 1**a. The concentrated graphene oxide (GO) dispersion was poured into the polytetrafluoroethylene (PTFE) mould, and dried at room temperature. After that, the GO film was peeled and heated in nitrogen atmosphere at 300 °C for 2 h with a heating rate of 3 °C min^{-1}. By using this simple technique, we are able to produce BHGF with A4 paper size (Figure 1b), this size being limited only by the size of the PTFE mould available. Moreover, the freestanding film shows good flexibility (Figure 1c) and can be easily cut into the desired shape (Figure 1d), which are highly desirable for emulating human skin.[18,29,30] After thermal treatment at 300 °C, the transformation from GO to conductive reduced graphene oxide (rGO) was confirmed by X-ray diffraction (XRD) and X-ray photoelectron spectroscopy (XPS).

In the XRD patterns, the BHGF exhibits a pronounced diffraction peak at 24.3° compared to 10° for GO (Figure 1e), indicating the partial removal of oxygen groups and showing some graphitic structure. XPS analysis reveals the C/O atomic ratio is increased from 1.92 for GO to 4.34 for BHGF, which is in good agreement with XRD analysis. High-resolution C1s spectrum of BHGF can be deconvoluted into five Gaussian peaks centered at 284.6, 285.4, 286.4, 287.9, and 289.2 eV, corresponding to the sp^2 C, sp^3 C, C—O, C═O, and O—C═O groups, respectively (Figure S1, Supporting Information).[31,32] Moreover, N_2 adsorption/desorption measurement of BHGF shows a low Brunauer–Emmett–Teller (BET) surface area of 13 m^2 g^{-1}, meaning its densely stacked graphene sheets.

Compared with the GO film with a dense structure (Figure 1f), scanning electron microscopy (SEM) image of the BHGF exhibits a honeycomb-like network that is assembled by multilayer-stacked graphene sheets (Figure 1g), and the pores are mainly derived from the volatilization of water remained in-between GO sheets during heat treatment. High-resolution SEM image further confirms high-density bubbles with the diameters ranging from 100 to 300 nm on the surfaces of graphene sheets, just like the bubble wrap (Figure 1h).

We proposed the formation mechanism of the BHGF as shown in **Figure 2**. During the thermal treatment

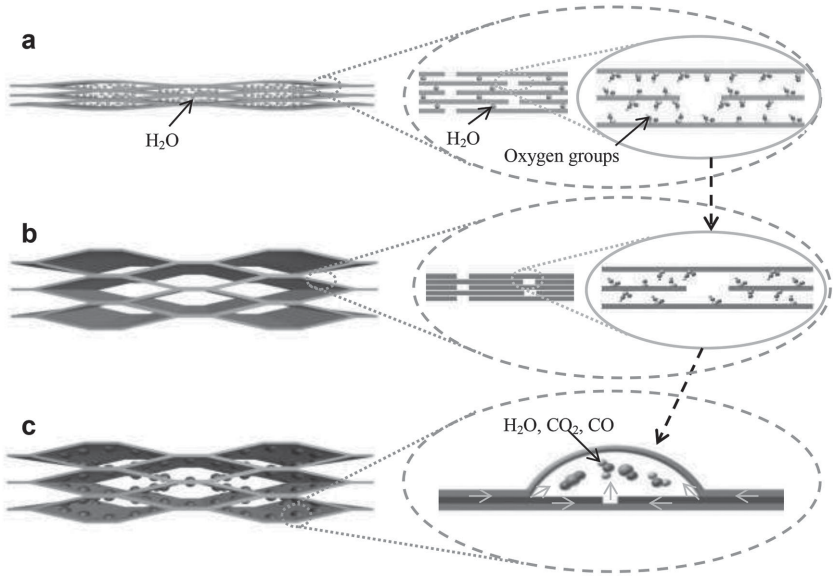

Figure 2. Schematic illustration of formation mechanism of the BHGF. a) Water trapped in the GO film. b) The formation of honeycomb-like network after the removal of water. c) The formation of bubbles on the sheets due to the evolved gases (H_2O, CO_2, and CO) trapped in adjacent graphene sheet.

below 150 °C, interlayer water remained in-between GO film would evaporate (Figure 2a), resulting in the formation of a honeycomb-like network (Figure 2b). Thermogravimetric analysis (TGA) shows about 15 wt% water remained in the dried GO film (Figure S2, Supporting Information). After that, the decomposition of oxygen-containing functionalities with temperature leads to small interlayer spacing of sheets (Figure 2b), and consequently numerous bubbles are formed on the surfaces of the graphene sheets (Figure 2c) due to the slowly evolved gases (H_2O, CO_2, and CO) trapped in adjacent graphene sheet. When the GO film is thermal-treated with a fast heating rate of 10 °C min^{-1}, the obtained reduced GO exhibits a worm-like morphology similar to expanded graphite (Figure S3, Supporting Information). The fast decomposition of oxygen-containing functionalities leads to high gas diffusion rate, resulting in tremendous volume expansion of graphene sheets due to instantaneously released gas.

2.2. Mechanical and Piezoresistance Properties

As is expected, the BHGF exhibits superb compressive elasticity and responsivity. The BHGF can be compressed to at least 95% strain, and completely recover to its original shape in less than 1 s when the loading is removed (**Figure 3**a and Movie S1, Supporting Information). Figure 3b shows the cyclic compression test (ε = 50%) of BHGF for 200 loading/unloading cycles. Two distinct regions are observed during the loading process, namely, a linear elastic region at $\varepsilon < 30\%$ corresponding to bending of graphene blocks or walls, and a densification region at $\varepsilon > 30\%$ corresponding to densification of cells (marked by white dotted line in Figure 1g). For the first compression cycle, the nearly linear elastic region of the BHGF is up to 30% strain, much higher than those of other graphene monolith (≈up to 20%).[26] More interestingly, there is no obvious plastic deformation for BHGF after fatigue testing (Figure 3c), in comparison to 10%–20% for other elastomeric carbon foams,[33,34] demonstrating excellent structural robustness. This result is surprising, as most carbon-based

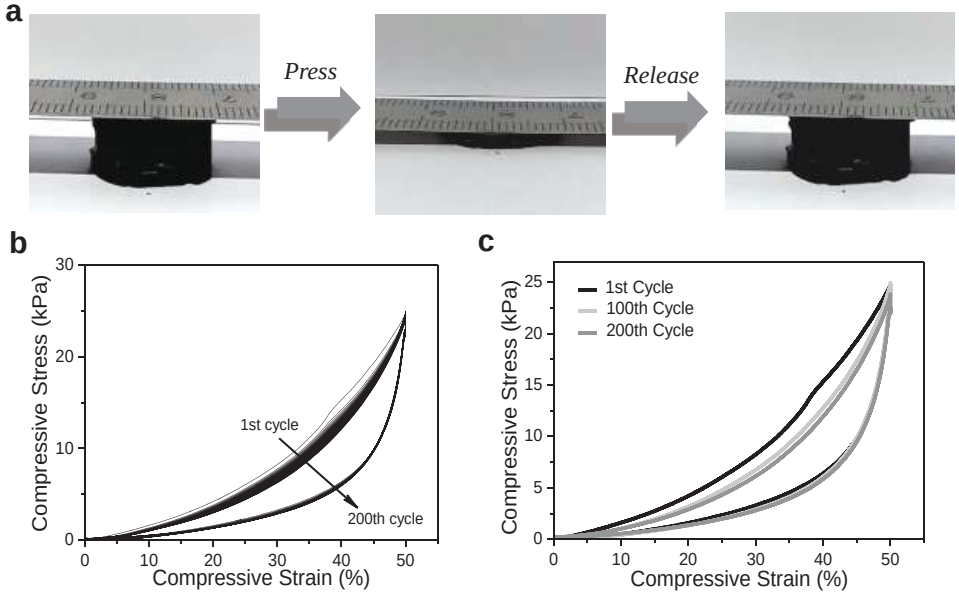

Figure 3. Compressive mechanical properties of the BHGF (seven-layer film). a) A set of real-time images of the compression–recovery process. b) Compressive fatigue test with ε = 50% for 200 cycles. c) Stress–strain curves of loading and unloading for 1st, 100th, and 200th cycle, respectively.

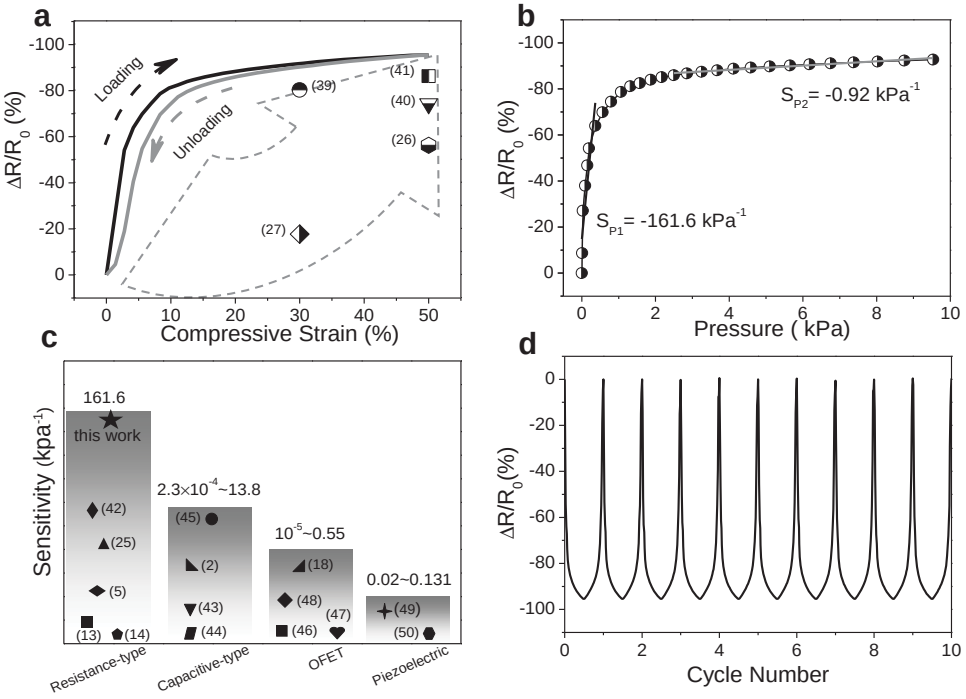

Figure 4. a) The relationship between $\Delta R/R_0$ and compressive strain of BHGF. The inseted symbols represent graphene monolith, graphene aerogel, 3D graphene sponge, and nanofiber-assembled cellular aerogel. b) The resistance variation ratio–pressure curve of BHGF; the BHGF shows a sensitivity of 161.6 kPa^{-1} in the low-pressure regime from 9 to 560 Pa. c) Comparison of pressure sensitivity of the BHGF pressure sensor with the resistance-type devices, capacitive-type devices, organic field-effect transistors, and piezoelectric devices. d) Resistance variation ratio recorded in the first ten loading/unloading cycles.

foams exhibit brittle manner when subjected to a large deformation.[35–38] Additionally, after 200 cycles, the maximum degradation of the BHGF under compressive stress is smaller than 3% (Figure 3c) and the bubble-like structure is still maintained (Figure S4, Supporting Information), further indicating remarkable structural stability.

The resistance variation ratios ($\Delta R/R_o = (R - R_o)/R_o$, where R_o represents the initial resistance) of the BHGF film with compressive strain are shown in **Figure 4**a. It can be clearly seen that there are three different regions on the loading curve such as high response region ($\varepsilon < 4\%$), transition region ($4\% < \varepsilon < 10\%$), and low response region ($10\% < \varepsilon < 50\%$). Notably, the BHGF exhibits higher resistance variation ratio at low strain than previously reported material.[26,27,39–41] Even at a strain of 20%, the BHGF still delivers a high resistance variation of 84%. Different from BHGF pressure sensors, the resistance–response of graphene foam shows an inverse curve (Figure S5, Supporting Information), the maximum resistance variation of graphene foam is 13%, much less than that of BHGF (89%). Moreover, the resistance variation ratio of BHGF can return to original values under loading–unloading process, indicating excellent mechanical stability and elasticity. This phenomenon has also been confirmed by relaxation and steady-state curve of BHGF sensor under loading (100 g weight, 5 s) and unloading process (Figure S6, Supporting Information). It is worth noting that BHGF possesses short relaxation time and excellent resistance–response, which are of benefit to pressure sensors.[18] All results show that BHGF can be suitably used as flexible, highly sensitive, and stable pressure sensors for various applications, in particular for electronic artificial skin.

The pressure sensitivity S_p (defined as $S_p = \delta\ (\Delta R/R_0)/\delta_p$) of the BHGF is calculated from the $\Delta R/R_o$–pressure curve as shown in Figure 4b. There are two apparent different piezoresistive sensitivities in the low and high-pressure regions. Remarkably, the BHGF shows an ultrahigh sensitivity as high as 161.6 kPa^{-1} in the low-pressure regime from 9 to 560 Pa corresponding to the strains less than 4% (Figure 3c), about 621 and 489 times higher than graphene–polyurethane sponge[14] and polypyrrole/silver hybrid sponge,[13] respectively. The sensitivity of the BHGF sensor is higher than the resistance-type devices (0.26–15.1 kPa^{-1}),[5,25,42] capacitive-type devices (2.3×10^{-4}–13.8 kPa^{-1}),[2,43–45] organic field-effect transistors (10^{-5}–0.55 kPa^{-1}),[18,46–48] and piezoelectric sensors devices (0.02–0.131 kPa^{-1})[49,50] (Figure 4c). More importantly, the resistive variation of 10% can be detected under a very low pressure of 9 Pa, which is very suitable for application in electronic skin. Figure 4d shows the resistance variation of the BHGF sensor at a strain of 50% in the first ten loading/unloading cycles. The loading/unloading curves are symmetrical and sharp, even after 200 cycles, the resistance–response curve shape is still maintained (Figure S7, Supporting Information), meaning excellent recovery property and high sensitivity of pressure sensor. Therefore, the electrical conductivity of the BHGF is highly sensitive to the pressure, thereby making it potential applications in highly sensitive pressure sensors and electronic artificial skin.

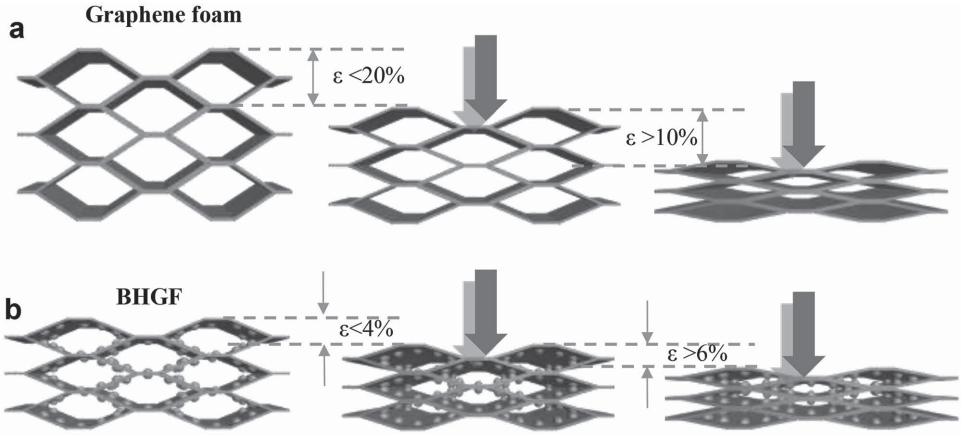

Figure 5. Pressure-sensing mechanism of graphene foam and BHGF. a) Structure change of graphene foam during the compression process. b) Obvious resistance variation of BHGF at low strain.

Recently, 3D MGMs with various structures such as foams,[51] sponges,[52] and aerogels,[53–55] have found broad applications in absorbents, catalysis, sensors, and energy storage and conversion.[56,57] Owing to the combination of 3D porous structure, excellent electric conductivity, and compressive elasticity, MGMs are considered as promising component for piezoresistive sensors.[58] Indeed, the piezoresistive sensitivity of MGMs is related to the densification of pore walls constructed by graphene skeleton, which depends on the thicknesses of pore walls, pore sizes and distribution, and weight density.[26,27] The pressure-sensing mechanism is determined by the structure change of sensors from completely disordered foam to perfectly ordered structure during the compression as shown in **Figure 5**. At a low strain less than 20% (Figure 5a), the resistive variation is related to the bending of stacked graphene sheets. Therefore, the resistance variation is very low due to the existence in an interconnected conductive structure during the densification of MGMs. Only at a strain higher than 30%, the more densification of the sheets is, the higher variation in conductivity is obtained. In the case of BHGF, the honeycomb structure is derived from the remaining water in-between stacked graphene sheets (Figure 5b). Under a very low strain, the pore walls would begin to contact with "point-to-point" and "point-to-face" modes, resulting in greatly increased conductivity of the film. At a higher strain, the resistance variation would gradually decrease because the nanosheets are in close contact with each other.

2.3. Detection of Finger Movement and Wrist Pulses

For further realization of the potential application as electronic artificial skin, BHGF was located on the back side of the finger joint and wrist for human motion detection as shown in **Figure 6**. The applied voltage on the pressure sensor for monitoring finger motion ranges from 10 mV to 1 V, the output currents are proportional to the applied voltage (Figure 6a). The output signals appear and disappear with the bending and straightening of finger, which is ascribed to the result of the different compression strain (Figure 6b). It is worth mentioning that our pressure sensor can be well driven even at a very low voltage of 10 mV, much lower than those of organic thin-film transistors (>6 V),[28] organic field-effect transistors (6 V),[48] and flexible polymer transistors (>10 V).[2] The low operating voltage of 10 mV of BHGF sensor is sufficiently low to allow for powering by energy-harvesting devices,[59] such as triboelectric generators.[60,61] Moreover, the signal amplitude also depends on the strain created by the finger bending. The more the finger bends, the more signal amplitude increases, as shown in Movie S2 (Supporting Information). Therefore, the pressure sensor performs perfectly after repeated finger motions, indicating good durability and flexibility.

To further detect slight variations in pressure on the strain sensor, we developed a wrist-wear device to monitor a human pulse (Figure 6c). By applying a voltage of 1 V on the pressure sensor, the pulses can be numbered by the successive signal amplitude. It is worth noting that the output signals exhibit good reproducibility, which is coincident with a young person's pulse (75 beats min^{-1}). We show that high-performance pressure sensors can be produced in a low-cost, facile, and scalable manner. Therefore, the above results demonstrate that the human pulse could be identified with our graphene-based pressure sensor, indicating that it is a potential wrist-wear device for detecting human's health.

3. Conclusion

In summary, we report a novel strategy for the fabrication of highly sensitive pressure sensor based on the bubbles decorated on honeycomb-like film. Due to switching effect depended on "point-to-point" and "point-to-face" contact modes, the freestanding flexible graphene pressure sensor exhibits an ultrahigh sensitivity at a very low strain, and excellent cycling stability, which can monitor human motions such as finger bending and pulse. Moreover, the sensor has a low operating voltage of 10 mV that can be powered by energy-harvesting devices, such as triboelectric generators. Therefore, the high sensitivity, long cycling life, and large-scale fabrication of the graphene pressure sensors make it a promising candidate for manufacturing low-cost artificial skin.

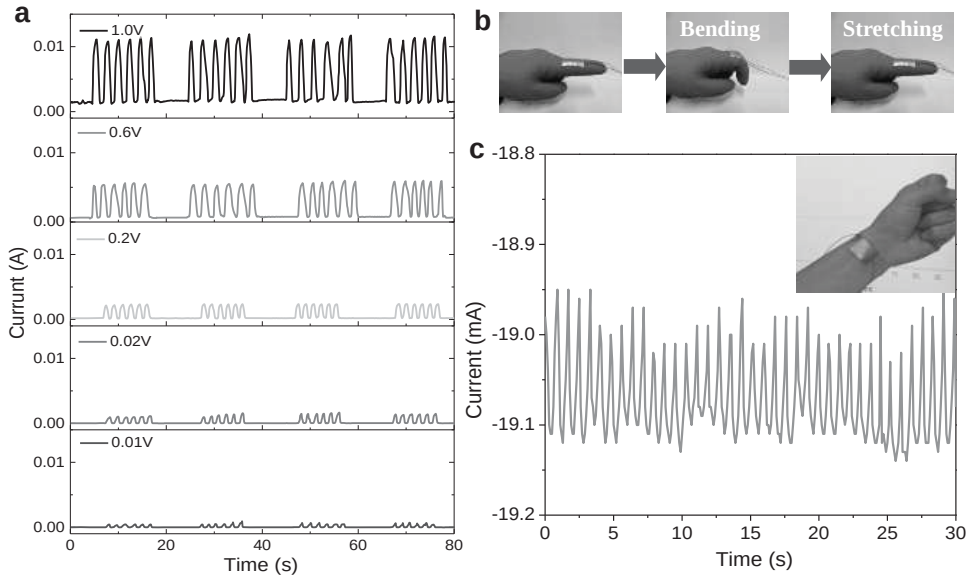

Figure 6. Wearable pressure sensor for detecting finger movement and pulse. a) The output signal amplitude of real-time finger motion under different voltages. b) Photographs of pressure sensor for monitoring the bending and straightening of finger. c) The output current signal of a young man's pulse; the inset image shows a pulse sensor for monitoring the physical force of a heartbeat in real time.

4. Experimental Section

Preparation of BHGF: GO was prepared by using a modified Hummers method, from natural graphite.[62] In this work, the concentration of GO suspension was designed to 4 mg mL^{-1}. First, the concentrated GO suspension was poured into the PTFE mould and smoothed by a glass rod. Second, the wet film was dried at room temperature for 12 h. Finally, the dried GO film was heated in nitrogen atmosphere at 300 °C for 2 h with a heating rate of 3 °C min^{-1}, and the obtained graphene film was named as BHGF. For comparison, graphene foam was prepared according to the following steps: First, 10 mL of 6 mg mL^{-1} GO aqueous suspension was sealed in a 16 mL Teflon autoclave and maintained at 180 °C for 12 h. Then the autoclave was naturally cooled to room temperature and the as-prepared gel was immersed in deionized water for 1 h and lead water to fill into graphene pores. Finally, the graphene hydrogel was rapidly frozen by quenching in liquid nitrogen and then freeze dried to form graphene foam.

Characterization Methods: The microstructure and morphology were characterized by SEM (SU70-HSD). The crystallographic structures of the samples were determined by XRD equipped with Cu Kα radiation (λ = 0.15406 nm). XPS spectra of the samples were measured by a Perkin-Elmer PHI-5700 ESCA system with a monochromated Al Kα X-ray source (1486.6 eV). The specific surface area was determined by the BET method using an N_2 gas adsorption analyzer (Quantachrome, NOVA 2000, USA). TGA was conducted with a differential thermal analyzer (STA 449 F3) from room temperature to 800 °C, and the heating rate was set at 10 °C min^{-1}. The compressive tests were carried out by using an AGS-X material testing system (SHIMADZU). The strain rate for 1 cm gauge length is 9 mm min^{-1} with a preload of 0.5 N. The electric test was performed on a CHI 660E potentiostat–galvanostat (CH Instruments Inc. Shanghai).

Pressure Sensor Fabrication and Measurement: The samples used were cut into square shaped films with a size of 5 × 5 cm^2. The seven square-shaped graphene films were sandwiched between two parallel metal electrodes; after that, the samples were placed on AGS-X material testing system (SHIMADZU) and kept at a preselected constant pressure, while the electrical response was simultaneously recorded by CHI 660E electrochemical workstation.

Wearable Pressure Sensor Fabrication and Measurement: The BHGF films were assembled into a resistive-type pressure sensor by sandwiching the film between two copper foils. The sizes of the BHGF film were 1 × 2 cm^2 for monitoring the bending and straightening of finger, and 1 × 1 cm^2 for wrist-wear device. The BHGF sensor was attached onto a person's finger joint and wrist by using duct tape, and connected to the measurement system with the CHI 660E electrochemical workstation.

Supporting Information

Supporting Information is available from the Wiley Online Library or from the author.

Acknowledgements

L.S. and Y.L. contributed equally to this work. The authors acknowledge financial support from Fundamental Research funds for the Central Universities (HEUCFD1411), Natural Science Foundation of Heilongjiang Province (E201416).

Received: July 17, 2015
Revised: August 14, 2015
Published online: September 23, 2015

[1] C. Pang, G. Y. Lee, T. I. Kim, S. M. Kim, H. N. Kim, S. H. Ahn, K. Y. Suh, *Nat. Mater.* **2012**, *11*, 795.
[2] G. Schwartz, B. C. Tee, J. Mei, A. L. Appleton, H. K. Do, H. Wang, Z. Bao, *Nat. Commun.* **2013**, *4*, 1859.
[3] L. Y. Chen, B. C. Tee, A. L. Chortos, G. Schwartz, V. Tse, D. J. Lipomi, H. S. Wong, M. V. McConnell, Z. Bao, *Nat. Commun.* **2014**, *5*, 5028.
[4] X. Liao, Q. Liao, X. Yan, Q. Liang, H. Si, M. Li, H. Wu, S. Cao, Y. Zhang, *Adv. Funct. Mater.* **2015**, *25*, 2395.
[5] X. Wang, Y. Gu, Z. Xiong, Z. Cui, T. Zhang, *Adv. Mater.* **2014**, *26*, 1336.
[6] R. Li, B. Nie, P. Digiglio, T. Pan, *Adv. Funct. Mater.* **2014**, *24*, 6195.

[7] B. C. K. Tee, A. Chortos, R. R. Dunn, G. Schwartz, E. Eason, Z. Bao, *Adv. Funct. Mater.* **2014**, *24*, 5427.
[8] K. Takei, T. Takahashi, J. C. Ho, H. Ko, A. G. Gillies, P. W. Leu, R. S. Fearing, A. Javey, *Nat. Mater.* **2010**, *9*, 821.
[9] A. P. Gerratt, H. O. Michaud, S. P. Lacour, *Adv. Funct. Mater.* **2015**, *25*, 2287.
[10] X. Wu, Y. Ma, G. Zhang, Y. Chu, J. Du, Y. Zhang, Z. Li, Y. Duan, Z. Fan, J. Huang, *Adv. Funct. Mater.* **2015**, *25*, 2138.
[11] L. Gao, Y. Zhang, V. Malyarchuk, L. Jia, K. I. Jang, R. C. Webb, H. Fu, Y. Shi, G. Zhou, L. Shi, D. Shah, X. Huang, B. Xu, C. Yu, Y. Huang, J. A. Rogers, *Nat. Commun.* **2014**, *5*, 4938.
[12] L. Pan, A. Chortos, G. Yu, Y. Wang, S. Isaacson, R. Allen, Y. Shi, R. Dauskardt, Z. Bao, *Nat. Commun.* **2014**, *5*, 3002.
[13] W. He, G. Li, S. Zhang, Y. Wei, J. Wang, Q. Li, X. Zhang, *ACS Nano* **2015**, *9*, 4244.
[14] H. B. Yao, J. Ge, C. F. Wang, X. Wang, W. Hu, Z. J. Zheng, Y. Ni, S. H. Yu, *Adv. Mater.* **2013**, *25*, 6692.
[15] W. Cai, Y. Huang, D. Wang, C. Liu, Y. Zhang, *J. Appl. Polym. Sci.* **2014**, *131*, 39778.
[16] F. Deng, M. Ito, T. Noguchi, L. Wang, H. Ueki, K.-I. Niihara, Y. A. Kim, M. Endo, Q.-S. Zheng, *ACS Nano* **2011**, *5*, 3858.
[17] Z.-M. Dang, M.-J. Jiang, D. Xie, S.-H. Yao, L.-Q. Zhang, J. Bai, *J. Appl. Phys.* **2008**, *104*, 024114.
[18] S. C. Mannsfeld, B. C. Tee, R. M. Stoltenberg, C. V. Chen, S. Barman, B. V. Muir, A. N. Sokolov, C. Reese, Z. Bao, *Nat. Mater.* **2010**, *9*, 859.
[19] L. Persano, C. Dagdeviren, Y. Su, Y. Zhang, S. Girardo, D. Pisignano, Y. Huang, J. A. Rogers, *Nat. Commun.* **2013**, *4*, 1633.
[20] S. Gong, W. Schwalb, Y. Wang, Y. Chen, Y. Tang, J. Si, B. Shirinzadeh, W. Cheng, *Nat. Commun.* **2014**, *5*, 3132.
[21] K. S. Kim, Y. Zhao, H. Jang, S. Y. Lee, J. M. Kim, K. S. Kim, J. H. Ahn, P. Kim, J. Y. Choi, B. H. Hong, *Nature* **2009**, *457*, 706.
[22] D. J. Cohen, D. Mitra, K. Peterson, M. M. Maharbiz, *Nano Lett.* **2012**, *12*, 1821.
[23] Y. Yang, H. Zhang, Z.-H. Lin, Y. S. Zhou, Q. Jing, Y. Su, J. Yang, J. Chen, C. Hu, Z. L. Wang, *ACS Nano* **2013**, *7*, 9213.
[24] F.-R. Fan, L. Lin, G. Zhu, W. Wu, R. Zhang, Z. L. Wang, *Nano Lett.* **2012**, *12*, 3109.
[25] C. L. Choong, M. B. Shim, B. S. Lee, S. Jeon, D. S. Ko, T. H. Kang, J. Bae, S. H. Lee, K. E. Byun, J. Im, Y. J. Jeong, C. E. Park, J. J. Park, U. I. Chung, *Adv. Mater.* **2014**, *26*, 3451.
[26] L. Qiu, J. Z. Liu, S. L. Chang, Y. Wu, D. Li, *Nat. Commun.* **2012**, *3*, 1241.
[27] Y. Li, J. Chen, L. Huang, C. Li, J. D. Hong, G. Shi, *Adv. Mater.* **2014**, *26*, 4789.
[28] Y. Zang, F. Zhang, D. Huang, X. Gao, C. A. Di, D. Zhu, *Nat. Commun.* **2015**, *6*, 6269.
[29] C. Hou, H. Wang, Q. Zhang, Y. Li, M. Zhu, *Adv. Mater.* **2014**, *26*, 5018.
[30] C. Wu, X. Huang, X. Wu, R. Qian, P. Jiang, *Adv. Mater.* **2013**, *25*, 5658.
[31] J.-Q. Huang, T.-Z. Zhuang, Q. Zhang, H.-J. Peng, C.-M. Chen, F. Wei, *ACS Nano* **2015**, *9*, 3002.
[32] C.-M. Chen, Q. Zhang, M.-G. Yang, C.-H. Huang, Y.-G. Yang, M.-Z. Wang, *Carbon* **2012**, *50*, 3572.
[33] X. Wang, L. L. Lu, Z. L. Yu, X. W. Xu, Y. R. Zheng, S. H. Yu, *Angew. Chem. Int. Ed. Engl.* **2015**, *54*, 2397.
[34] H. W. Liang, Q. F. Guan, L. F. Chen, Z. Zhu, W. J. Zhang, S. H. Yu, *Angew. Chem. Int. Ed. Engl.* **2012**, *51*, 5101.
[35] A. M. Elkhatat, S. A. Al-Muhtaseb, *Adv. Mater.* **2011**, *23*, 2887.
[36] Y. Gogotsi, *Science* **2010**, *330*, 1332.
[37] F. Yavari, Z. Chen, A. V. Thomas, W. Ren, H. M. Cheng, N. Koratkar, *Sci. Rep.* **2011**, *1*, 166.
[38] Y. Xu, K. Sheng, C. Li, G. Shi, *ACS Nano* **2010**, *4*, 4324.
[39] J. Li, J. Li, H. Meng, S. Xie, B. Zhang, L. Li, H. Ma, J. Zhang, M. Yu, *J. Mater. Chem. A* **2014**, *2*, 2934.
[40] Y. Si, J. Yu, X. Tang, J. Ge, B. Ding, *Nat. Commun.* **2014**, *5*, 5802.
[41] J. Li, S. Zhao, G. Zhang, Y. Gao, L. Deng, R. Sun, C. Wong, *J. Mater. Chem. A* **2015**, 2934.
[42] J. Park, Y. Lee, J. Hong, M. Ha, Y.-D. Jung, H. Lim, S. Y. Kim, H. Ko, *ACS Nano* **2014**, *8*, 4689.
[43] Q. Cao, S. H. Hur, Z. T. Zhu, Y. G. Sun, C. J. Wang, M. A. Meitl, M. Shim, J. A. Rogers, *Adv. Mater.* **2006**, *18*, 304.
[44] D. J. Lipomi, M. Vosgueritchian, B. C. Tee, S. L. Hellstrom, J. A. Lee, C. H. Fox, Z. Bao, *Nat. Nanotechnol.* **2011**, *6*, 788.
[45] Y. Shu, H. Tian, Y. Yang, C. Li, Y. Cui, W. Mi, Y. Li, Z. Wang, N. Deng, B. Peng, T. L. Ren, *Nanoscale* **2015**, *7*, 8636.
[46] G. Darlinski, U. Böttger, R. Waser, H. Klauk, M. Halik, U. Zschieschang, G. N. Schmid, C. Dehm, *J. Appl. Phys.* **2005**, *97*, 093708.
[47] I. Manunza, A. Sulis, A. Bonfiglio, *Appl. Phys. Lett.* **2006**, *89*, 143502.
[48] T. Someya, T. Sekitani, S. Iba, Y. Kato, H. Kawaguchi, T. Sakurai, *Proc. Natl. Acad. Sci. USA* **2004**, *101*, 9966.
[49] W. Wu, X. Wen, Z. L. Wang, *Science* **2013**, *340*, 952.
[50] A. V. Shirinov, W. K. Schomburg, *Sens. Actuators, A* **2008**, *142*, 48.
[51] M. Inagaki, J. Qiu, Q. Guo, *Carbon* **2015**, *87*, 128.
[52] X. Xu, Z. Sun, D. H. Chua, L. Pan, *Sci. Rep.* **2015**, *5*, 11225.
[53] H. Hu, Z. Zhao, W. Wan, Y. Gogotsi, J. Qiu, *Adv. Mater.* **2013**, *25*, 2219.
[54] H. Sun, Z. Xu, C. Gao, *Adv. Mater.* **2013**, *25*, 2554.
[55] H. Hu, Z. Zhao, Y. Gogotsi, J. Qiu, *Environ. Sci. Technol. Lett.* **2014**, *1*, 214.
[56] Z. Xu, H. Sun, C. Gao, *APL Mater.* **2013**, *1*, 030901.
[57] B. Luo, L. Zhi, *Energy Environ. Sci.* **2015**, *8*, 456.
[58] A. H. Lu, G. P. Hao, Q. Sun, *Angew. Chem. Int. Ed. Engl.* **2013**, *52*, 7930.
[59] V. Bhatnagar, P. Owende, *Energy Sci. Eng.* **2015**, *3*, 153.
[60] W. S. Jung, M. G. Kang, H. G. Moon, S. H. Baek, S. J. Yoon, Z. L. Wang, S. W. Kim, C. Y. Kang, *Sci. Rep.* **2015**, *5*, 9309.
[61] P. Bai, G. Zhu, Q. Jing, J. Yang, J. Chen, Y. Su, J. Ma, G. Zhang, Z. L. Wang, *Adv. Funct. Mater.* **2014**, *24*, 5807.
[62] L. Jiang, L. Sheng, C. Long, Z. Fan, *Nano Energy* **2015**, *11*, 471.